Pure Appl. Chem., Vol. 73, No. 10, pp. 1613–1623, 2001.

Ultrafast dynamics at solid/liquid interfaces as investigated by photothermal spectroscopy*

Tsuguo Sawada

Graduate School of Frontier Sciences, The University of Tokyo, Hongo, Bunkyo-ku, Tokyo 113-8656 Japan

Abstract: Among the recent topics of photothermal (PT) applications of lasers, we focus on ultrafast (≦1.0 ns) photothermal/photoacoustic (PT/PA) phenomena occurring at interfaces, which play important roles in nanoscale materials science and technology. Here, we describe our recently developed novel PT techniques called transient reflecting grating (TRG) spectrometries. These techniques have been applied to the studies of solid surfaces, film substrates, and solid/liquid interfaces.

INTRODUCTION

There is a wide variety of photothermal (PT), photoacoustic (PA), and related phenomena, because materials under light illumination always generate heat, which triggers these phenomena. The heat causes a rise in local temperature, the material expansion and acoustic wave emission, the refractive index change inside and outside the material, and so on. These PT/PA phenomena have been utilized for spectroscopic and analytical purposes including physical, physicochemical, and ultratrace analyses; nondestructive evaluation and thermophysical investigation; noncontact monitoring and biological, medical, agricultural, food, and environmental applications [1–3]. Some aspects of material processing as well as laser cleaning are deeply concerned with PT/PA phenomena as well.

Photothermal spectroscopy is advantageous in comparison with conventional absorption and fluorescence spectroscopies as described below. The optical energy absorbed by materials (including atoms and molecules) interacts with neighbor materials and generates heat. The physical changes (for example, change of refractive index, and so on) induced as the result of heat generation reflect strongly various information on both optically excited materials themselves and neighbors around the materials. This is a distinct characteristic of the photothermal spectroscopy.

Because light illumination triggers PT/PA phenomena, characteristics of the light, in conjunction with those of the material being illuminated, greatly influence what will happen on the target material. If we know optical, thermal, and elastic properties of the target material system, by using the coherent light of a laser, which is an ideal source of well-controlled temporal and spatial shapes as well as of spectral purity and high intensity, we can optically control temporal and spatial shapes of the heat and sound sources with a high degree of freedom. In turn, observation of heat and sound induced by laser illumination can provide valuable information about the molecular and material properties of the sample, as numerous studies have demonstrated [1–3]. Beyond these, use of the latest generation of lasers with high-performance optical equipment for PT observations gives rise to an increasing number of chances to answer fundamental questions directly concerned with atomic-, molecular- and mesoscopic-scale PT phenomena in condensed media. It is possible to achieve a detection limit for nonlumines-

*Lecture presented at the IUPAC International Congress on Analytical Sciences 2001 (ICAS2001), Tokyo, Japan, 6–10 August 2001. Other presentations are published in this issue, pp. 1555–1623.

cent molecules at a single molecule level [4], to count a single 10-nm Ag particle undergoing Brownian motion in liquid [5], to observe heat generation of a few picoseconds from molecules in solution [6,7], to generate and detect the terahertz acoustic pulse of a several-nanometer wavelength in an ultrathin metallic film [8], and to observe subpicosecond heat generation at solid/liquid interfaces [9]. Some of the findings go beyond PT/PA phenomena and overlap with other fields of science, with implications for single-molecule spectroscopy [10], ultrafast dynamics of molecules [11], laser ultrasonics [12], and femtochemistry at surfaces [13,14].

Among the recent topics of PT application of lasers, we focus on fast and ultrafast PT/PA phenomena occurring at interfaces, especially at electrochemical interfaces of metals and aqueous solutions. (In this review, we distinguish as *fast* the PT/PA phenomena as faster than 10 ns, which until the latter half of the 1980s was thought to be the resolution limit of PT/PA detection, and we use *ultrafast* in the same sense as with ultrafast spectroscopy.) Investigations of solid surfaces, film-substrate systems, and liquid/solid interfaces have provided the unique and practical applications of PT/PA techniques, which are capable of nondestructive depth profiling of an opaque material and its over-layers [15]. As heat can diffuse a finite distance in a finite time interval, we can expect higher depth resolutions with higher temporal resolutions in PT depth profiling. For an interface under ultrafast PT observation, the thickness of the system being investigated can be reduced to a size of a molecule. We also bring to the readers' attention some of the exciting experimental and theoretical results from fast and ultrafast PT/PA measurements of the solid/liquid interfaces. We show how ultrafast PT/PA phenomena are measured and how they have been applied, or will be in the future, to studies of the interfaces.

Here, we summarize recent studies on ultrafast energy transfer at solid/liquid interfaces, focusing on our newly developed photothermal techniques: femtosecond transient reflectivity (fs-TR) method, femtosecond transient reflecting grating (fs-TRG) method, and transient reflecting grating spectrometry (TRGS). Firstly, Pt/aqueous electrolyte interfaces were measured using the fs-TR method. An ultrafast relaxation component of 20 fs was first observed in the Pt/HCl (aq) and Pt/H_2SO_4 (aq) interfaces, in which the anions (Cl^- and SO_4^{2-}) have strong affinity to the Pt surface. It was suggested that this is due to the scattering of nonthermalized electrons by adsorbed anions. Secondly, TiO_2/KSCN (aq) interfaces were measured using the fs-TRG method. Ultrafast relaxation components (110–690 fs) were observed in the TRG signals. This marked the first observation of the contribution of nonequilibrium holes to the energy transfer at TiO_2/KSCN (aq) interfaces. Thirdly, the TRGS method will be briefly described, focusing on both the spectroscopic behavior of hot electrons and thermal diffusion. The results indicated that ultrafast energy transfer processes occur prior to the heat diffusion, and this process is hindered by the adsorbed ions.

OBSERVATION OF ULTRAFAST RELAXATION PROCESS AT PT/ELECTROLYTE INTERFACES BY FEMTOSECOND TRANSIENT REFLECTIVITY (TR) METHOD

Firstly, transient reflectivity measurement was performed in order to obtain information on ultrafast dynamics at solid/liquid interfaces. The transient reflectivity (TR) method simply monitors transient reflectivity change induced by a pump beam using a probe beam [16]. When a sample surface is irradiated by the pump beam, electronic excitation occurs in the irradiated spot. The excitation brings about refractive index change, i.e., reflectivity change. Therefore, information on electronic excitation can be obtained by monitoring the intensity of the reflected light of the probe beam. By using a femtosecond pulsed laser with an autocorrelation of 170 fs, the method was successfully extended to a 10-fs time region. Details on the experimental setup have been described in our previous review [17].

We measured TR for a polycrystalline Pt thin-film with a thickness of 30 nm immersed in aqueous electrolyte solutions, focusing on the interfacial electronic interaction between Pt and anions (Fig. 1) [16]. By using the thin-film instead of bulk Pt, the diffusion of hot electrons perpendicular to the interface could be prevented. Three types of aqueous electrolyte solutions were used for the meas-

urement: 0.1 mol dm^{-3} $HClO_4$, 0.1 mol dm^{-3} H_2SO_4, and 0.1 mol dm^{-3} HCl. Since the affinities of Cl^- and SO_4^{2-} to a Pt thin-film are stronger than that of ClO_4^-, the effect of affinity to the ultrafast dynamics could be investigated.

Figure 2 shows TR responses at the Pt/electrolyte solution interfaces. The ratio of reflectivity change ($\delta R/R$) is on the order of 10^{-5} to 10^{-4}. The curves in Fig. 2 correspond to the following processes. Electrons within the optical penetration depth (less than 15 nm) are excited, and subsequently the excited electrons are thermalized within 1 ps. The reflectivity change within 1 ps corresponds to an energy transfer process from the electrons to the Pt lattice by way of electron-phonon coupling, and that after thermalization corresponds to electron temperature.

The analysis of the curves was performed considering instrumental functions. It was found the bi-exponential model was only valid for the TR responses for pure water and $HClO_4$. The TR responses for HCl and H_2SO_4 were suitably fitted with a tri-exponential model. The fitting parameters are summarized in Table 1. The first and second components correspond to the electron-phonon coupling relaxation and heat diffusion, respectively. The relaxation times of electron-phonon coupling agree with those reported in an early work of the Pt surface in the UHV [18]. On the other hand, the third component (20 fs) in HCl and H_2SO_4 solutions was first observed in this study. The relaxation time 20 fs is much faster than the processes of electron-phonon coupling, and mechanisms faster than the electron-phonon coupling should be considered. It is natural to consider that this component reflects the strong affinity of the anions to the Pt surface. It is proposed that the third component is due to nonradiative relaxation of nonthermalized electrons (NTEs) through interfacial scattering by adsorbed anions. The NTEs are the electrons that are not in equilibrium with other electrons below the Fermi level, i.e., they

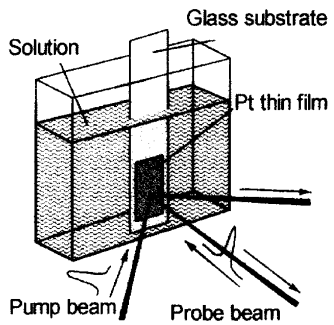

Fig. 1 Schematic illustration of the experimental arrangement around the sample cell for femtosecond time-resolved transient reflectivity measurements. The Pt thin film was 30 nm thick, and aqueous solutions used were 0.1 M $HClO_4$, 0.1 M HCl, 0.1 M H_2SO_4, and pure water.

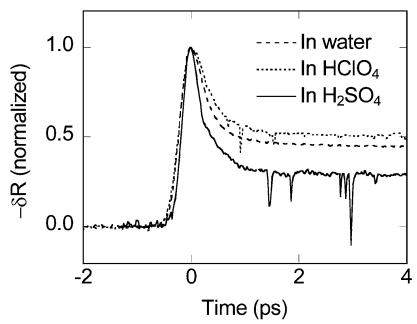

Fig. 2 Transient reflectivity responses at the Pt/aqueous electrolyte solutions interfaces.

Table 1 Time constants and pre-exponential factors calculated as fitting parameters for the transient reflectivity responses from Pt/aqueous electrolyte solutions interfaces.

	τ_1 (ps)	τ_2 (ps)	τ_3 (ps)	C_1	C_2	C_3
Pure water	0.3	60		0.72	0.28	
$HClO_4$	0.4	100		0.66	0.34	
HCl	0.6	100	0.02	0.03	0.02	0.95
H_2SO_4	0.7	100	0.02	0.03	0.02	0.95

do not follow the Fermi distribution. The NTEs are first excited by incident photons, and they scatter with other electrons to attain the Fermi distribution. It is considered that this process is affected by the adsorbed anion and appeared as the third process.

In summary, the Pt/electrolyte interfaces were measured using the femtosecond TR method. A novel ultrafast relaxation component (20 fs) was found in the Pt/HCl (aq) and Pt/H_2SO_4 (aq) interfaces. It was proposed that this is due to the scattering of nonthermalized electrons by adsorbed anions.

FEMTOSECOND TRANSIENT REFLECTING GRATING (TRG) METHOD AND ITS APPLICATION TO MONITORING OF ULTRAFAST ENERGY TRANSFER AT TiO_2/KSCN (aq) INTERFACES

As described in the preceding section, the TR method monitors extremely small reflectivity changes ($\delta R/R = 10^{-5} - 10^{-4}$). This causes low S/N ratio of the TR signals and experimental difficulties in measurements. In order to improve S/N ratio of the ultrafast signals, we developed a femtosecond transient reflecting grating (TRG) method and successfully applied it to solid/liquid interfaces [19,20].

The principle of the transient reflecting grating (TRG) method is shown in Fig. 3. Two pump pulses of the same wavelength λ_{pump} cross on a sample surface, to form an optical interference pattern with a fringe spacing Λ, $\Lambda = \lambda_{pump} / 2\sin\theta$ where θ is a pump beam incident angle normal to the surface. This interference pattern transforms into a periodical refractive index change, which acts as a transient diffraction grating. A probe pulse is incident normal to the grating, and a diffracted light is observed. The intensity of the diffracted light is monitored as a function of the delay time of the probe beam. The TRG signal reflects dynamic information on surfaces, such as refractive index change by electronic excitation and heat generation.

The experimental setup for the TRG method is shown in Fig. 4. The light source was a regeneratively amplified Ti:Sapphire laser system which had an auto-correlation of 150 fs, wavelength of 800 nm, and repetition rate of 1 kHz.

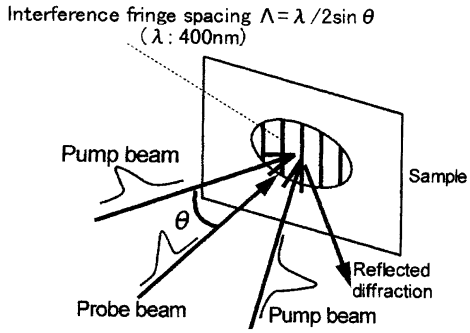

Fig. 3 Schematic illustration of the principle of the TRG method. Two pump laser pulses excite an interference fringe at the intersection, which acts as a transient reflecting grating for a probe beam.

A sample cell was fabricated for solid/liquid interface measurements. Its optical window was made of quartz glass with optically flat surfaces, and the thickness of the liquid phase could be controlled by changing the spacers. Controlling the thickness of the liquid phase was indispensable to improving the S/N ratio, because fluctuation of the liquid phase greatly disturbs the measurement. A solid/liquid interface was prepared by pouring a KSCN (aq) solution into the sample cell. A TiO_2 single crystal was attached to the sample cell. We intended to study how the population of adsorbate on TiO_2 affects the behavior of photoexcited carriers.

TRG responses from the interfaces between TiO_2 and KSCN (aq) in the range of 0–20 mM are shown in Fig. 5. As the result of decreasing the thickness of the liquid phase, the intensity of the TRG signals was almost the same, regardless of the thickness of the liquid phase. This indicates that the TRG signals were not from the bulk solutions but from the interface.

An increase in the TRG signal corresponds to the change in the refractive index of the sample surfaces induced by the generation of photoexcited carriers. In Fig. 5, the small fall in TRG responses after

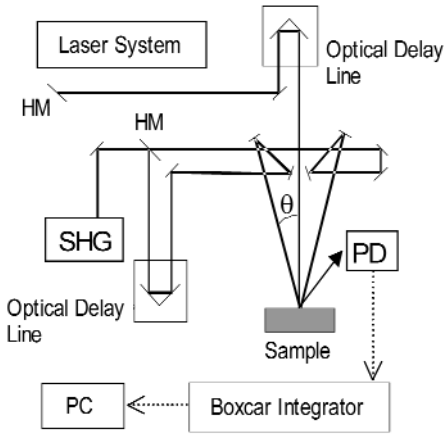

Fig. 4 Experimental setup for the femtosecond TRG method. HM, half mirror; PD, photodiode.

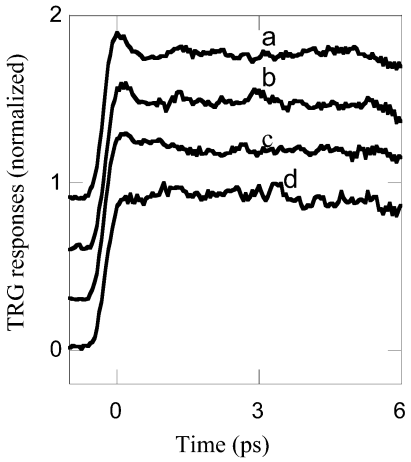

Fig. 5 Typical TRG signals from TiO_2/SCN^- aq interfaces with various SCN^- concentrations. The concentrations of SCN^- are as follows: a: 20 mM, b: 15 mM, c: 10 mM, and d: 0 mM. For clarity, the signals are vertically displaced.

the maximum becomes greater with increasing SCN^- concentration, and this small fall is never observed at the TiO_2/H_2O interface. The adsorption of SCN^- ion is not saturated in this concentration region, and the number of the adsorbate increases with increasing concentration of SCN^-. Therefore, the increase in the intensity of the small fall reflects the phenomena involving the adsorbate (SCN^-). The maximum height of the TRG signal is almost constant in all experiments, which suggests that there is no change in the density of pump beam fluency due to self-focusing induced by the SCN^- (aq). These facts indicate that an ultrafast relaxation process of the photoexcited holes (110–690 fs) occurs at the TiO_2/SCN^- (aq) interfaces.

Figure 6 shows the intensity of the ultrafast decay component vs. the concentration of SCN^-. The intensity of the ultrafast decay component increases with the increase of SCN^- concentration; that is, the ultrafast relaxation of the photoexcited holes becomes dominant with the increase in the number of adsorbed SCN^- ions. Thus, we can presume that the observed ultrafast decay (110–690 fs) is mainly due to ultrafast hole transfer at the interfaces.

Next, the photoexcited hole dynamics at several pump beam powers was considered. Figure 7 shows the dependence of the TRG responses from the TiO_2/SCN^- interfaces on the number of the photoexcited carriers. The concentration of the SCN^- (aq) is all 15 mM in this experiment. Since the atomic density of the TiO_2 is 100 times higher than that of the photoexcited carriers, the absorption by the

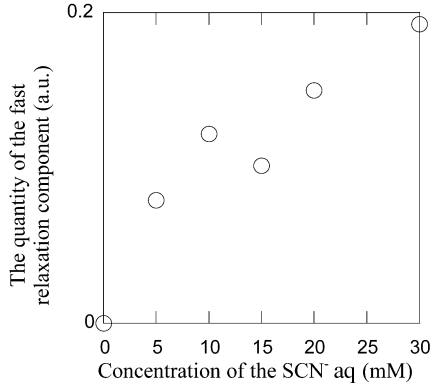

Fig. 6 Intensity of the ultrafast decay component vs. the concentration of SCN^-. The intensity of the component increases with increasing concentration of SCN^-.

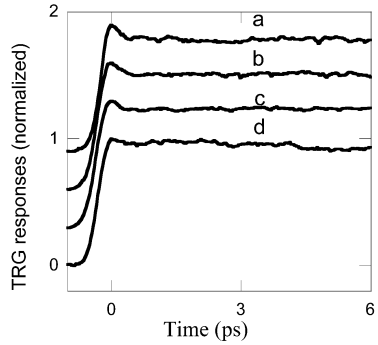

Fig. 7 Typical TRG signals from the TiO_2/SCN^- aq interfaces with various pump beam powers. The intensities of the pump beam power are as follows: a: 4 mW, b: 5 mW, c: 7 mW, d: 8 mW. For clarity, the signals are vertically displaced.

solid sample (TiO_2) is not saturated even at high power. The intensity of the TRG signals and the relative number of the photoexcited carriers which contribute to the interfacial reaction vs. the pump beam power is plotted in Fig. 8. The intensity of the TRG signals and the relative number of the photoexcited carriers increase with the increase of the pump beam power. However, the coefficients of the increase are not as expected. This means that the ratio of the ultrafast charge transfer decreases with an increasing number of photoexcited carriers. This is probably because the path for the ultrafast charge transfer is controlled by not only the density of photoexcited carriers but also other factors, such as the number of adsorbate molecules and the number of lattice defects at the interface.

The obtained TRG signals are fitted with a double exponential decay using a least-squares method, after deconvolution of an instrumental function. As shown in Table 2, the time constant increases with increasing the pump beam power (110–690 fs), whereas the intensity decreases with increasing the pump beam power. The increase in the time constants is probably due to the change in path for the ultrafast charge transfer as discussed above.

Photoexcited holes exist as nonequilibrium holes on a time scale of 100 fs after which they undergo an energy dissipation process via the carrier-carrier scattering. Our experimental results suggest a role for nonequilibrium holes in the reaction at the TiO_2/SCN^- interfaces. With the increase in the number of photoexcited carriers, the energy dissipation process becomes dominant and the interfacial reactive process occurs less, because the rate of the carrier-carrier scattering process increases, and vice versa. We believe this is the first observation of the contribution of nonequilibrium holes to the reaction at TiO_2/SCN^- interfaces. It is very exciting to note that the ultrafast nonequilibrium hole transfer in 110–690 fs was observed here, because it has been thought that nonequilibrium hole transfer does not occur and only equilibrated holes can be transferred across an interface. This work indicates that the

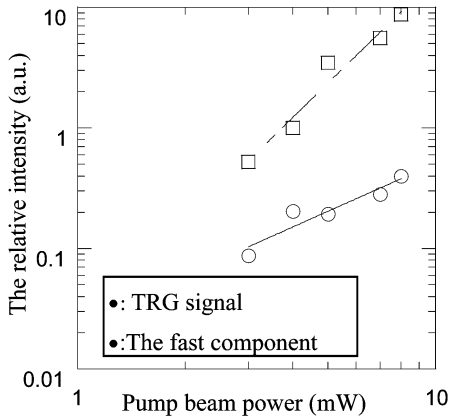

Fig. 8 Intensity of the TRG signals and the relative intensity of the fast relaxation component vs. pump beam power.

Table 2 Time constants and pre-exponential factors calculated as fitting parameters for the TRG signals from TiO_2/KSCN (aq) interfaces. Concentration of KSCN is fixed at 15 mM.

Pump power intensity (mW)	τ_1 (fs)	τ_2 (ps)	C_1	C_2
4	110	173	0.54	0.46
5	200	137	0.38	0.62
7	450	130	0.22	0.78
8	690	150	0.17	0.83

nonequilibrium holes should be taken into account in interface reactions. This result will provide valuable knowledge for designing electrode surfaces and controlling interfacial reactions.

DEVELOPMENT OF ULTRAFAST TRANSIENT REFLECTING GRATING SPECTROMETRY (TRGS)

A newly developed TRGS system is illustrated in Fig. 9. A regeneratively amplified titanium sapphire laser was used as a light source (800 nm, 1 kHz, pulse width 230 fs). The pulse was separated into pump and probe pulses using a partial reflective mirror. The pump pulses were frequency doubled to a wavelength of 400 nm (3.1 eV) and then further divided into two pulses by a half mirror. The two pump pulses were crossed and irradiated onto the same spot of the sample surface, to coincide in time to form an interference pattern. The pump intensity was less than 1 mJ/cm^2 per pulse at the sample. The probe pulse was focused to a 10-mm-thick cell filled with carbon tetrachloride to generate a femtosecond white light continuum after passing through a computer-controlled optical delay line. Wavelengths used ranged from 450 nm (2.75 eV) to 750 nm (1.91 eV). The probe pulse was irradiated at the center of the spot. The reflected diffracted light with a rainbow of colors spread like a fan owing to the diffraction conditions. It was directed to the entrance of the optical fiber end after being collected and focused by the lens. The sample was a vapor-deposited gold film 100 nm thick, prepared with a vacuum coater.

For the white light continuum used, interband transitions occur at wavelengths shorter than 640 nm, but not longer than this. Thus, comparison can be made between the signals for an interband transition and for an intraband transition. From detailed analyses of the gold band structure in the literature [21–24], we can suppose that two interband transitions are involved in the probe wavelength region and they correspond to d-band to Fermi surface transitions at X and L in the Brillouin zone. Their absorptions begin from 1.94 eV (640 nm) and 2.45 eV (507 nm), respectively. On the other hand, the pump pulse (400 nm: 3.1 eV) generates photoexcited carriers mainly only due to the L transition.

The TRG spectrum at each delay time is shown in Fig. 10. There are two peaks at 510 nm (2.5 eV) and 620 nm (2.0 eV), and the signal intensity rises to a maximum at 0.2 ps for every wave-

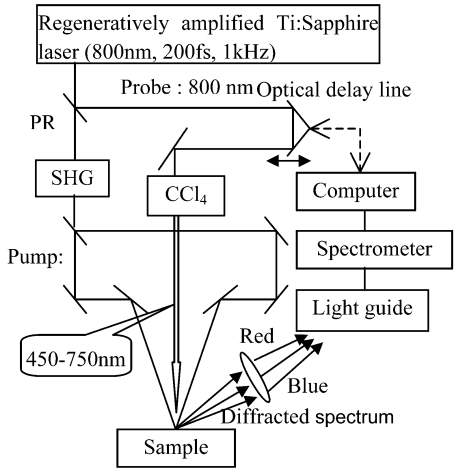

Fig. 9 Experimental arrangement for the transient reflecting grating method using a femtosecond white light continuum probe pulse. The probe pulse was focused to the 10-mm-thick cell filled with carbon tetrachloride to generate a femtosecond white light continuum (450–750 nm). The spread reflected diffracted light with a rainbow of colors was directed to the light guide after being focused by the lens. (PRM) partially relective mirror, (SHG) nonlinear.

length. The peaks at 510 and 620 nm show a different temporal tendency. It is clear that the former has a faster relaxation component. We may consider that the signal at each peak corresponds to an electron density change in the vicinity of the Fermi surface at X and L, because the position of each peak is in good agreement with each transition. The maximums of the two peaks are more than 5 times larger in intensity than at 700 nm, the wavelength for the intraband transition.

To clarify the signal decay, some TRG responses at typical wavelengths are shown in Fig. 11. This response shows a 10-ps linear decay, and the decay is observed for every wavelength. Compared with results in the literature, the linear decay corresponds to the temperature fall of photoexcited electrons can be considered to be due to electron-phonon scattering. It was proved using the two-temperature model that this component decays linearly, when the temperature of photoexcited electrons is much

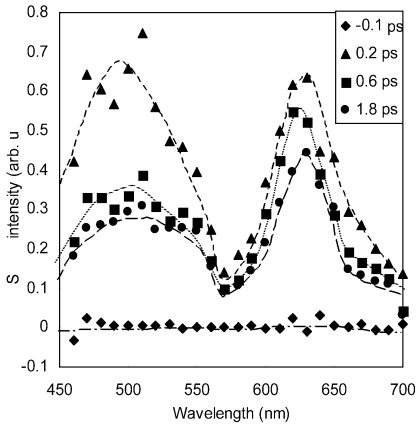

Fig. 10 Transient reflecting grating spectra at various probe delays. The measured sample was a vapor-deposited gold film (thickness: 100 nm). For clarity of the spectrum shape, a smooth line is also shown for each delay time.

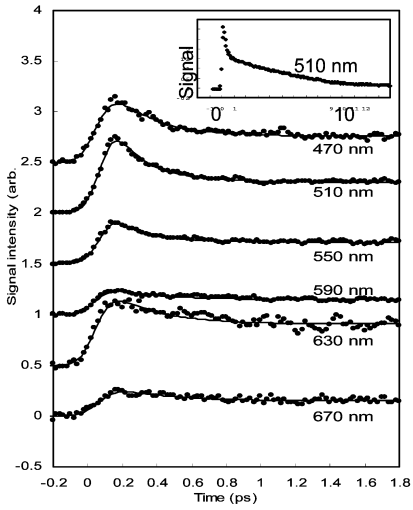

Fig. 11 Transient reflecting grating responses and fitted curves for various probe wavelength until 1.8 ps. Each waveform is vertically displaced for clarity. The measured sample was a vapor-deposited gold film (thickness: 100 nm). The inset shows a typical transient reflecting grating response until 15 ps (probe wavelength: 510 nm).

higher than that of phonons [25]. Looking at TRG responses within 1 ps, we observe two relaxation components around 510 nm, that is, the transition at L, while only the slower component is observed for every wavelength. The waveforms for every wavelength can be fitted with 40 ± 10 fs and 280 ± 40 fs. The ratio of 40-fs component in the waveforms increases as the wavelength gets nearer to 510 nm, and decreases moving away from it. For wavelengths longer than 550 nm, only the 280-fs component is included in the waveforms.

Since these relaxations occurred before electron-phonon coupling, we can suppose that the processes correspond to the thermalization due to electron-electron scattering (e-e scattering). A two-step relaxation like this result has never been observed. Then we reconsidered Fermi liquid theory, which has been used for an explanation of the thermalization processes. The thermalization time due to e-e scattering is predicted from theory as [26]

$$\frac{1}{\tau_e} = K\frac{\left(\pi k_B T_e\right)^2 + \varepsilon^2}{1+\exp(-\varepsilon / k_B T_e)} \tag{1}$$

where T_e is the electron temperature at the conduction band, ε is the energy of a focused electron measured from the Fermi energy, and K is the e-e scattering constant. Considering that the pump beams (3.11 eV) excite electrons around the transition at L (2.45 eV), ε equals 0.66 eV just after photoexcitation, which is much larger than $k_B T_e$, and then eq. 1 is approximated as $1/\tau_e \approx K\varepsilon^2$. When their energy is reduced to $k_B T_e$, eq. 1 is approximated as $1/\tau_e \approx K(\pi k_B T_e)^2$, which physically means available phase space in the energy range of $k_B T_e$. From these considerations, we now see that two processes are involved in the thermalization processes due to e-e scattering.

Using the above approximated equation, the relaxation time due to the faster e-e scattering is estimated to be 42 fs with $K = 0.055$ (eV/fs^{-1}) [27] and that due to the slower e-e scattering is calculated as 310 fs with the K and $\tau_e = 960$ K; τ_e is obtained from the absorbed energy per volume: 2.7×10^7 (Jm^{-3} pulse^{-1}) and the electronic specific heat: $66T_e$ (Jm^{-3}K^{-1}). We can conclude that the two observed relaxations correspond to the thermalization processes owing to the above-mentioned two kinds of e-e scattering, because of the good agreement between the theoretical and experimental time constants.

We note that the relaxation due to the faster e-e scattering is observed only around the transition at L, while the slower e-e scattering is observed for every wavelength. These results indicate that the faster e-e scattering occurs only around the L, while the NTEs dissipate their energy to other electrons to make other NTEs in various regions of the Brillouin zone. Thus, the slower e-e scattering is observed for every wavelength. We summarize the relaxation phenomena as follows: First, the pump beam (3.11 eV) excites electrons at the L point in the Brillouin zone to about 0.66 eV above the Fermi level. Secondly, the relaxation of NTEs occurs due to the faster e-e scattering in the vicinity of L and the dissipated energy is distributed to other electrons in various regions of the Brillouin zone (40 fs). Thirdly, the newly generated NTEs thermalize and show the Fermi distribution (280 fs). Finally, the raised temperature of the electrons falls due to electron-phonon scattering (10 ps).

CONCLUSION

In this article, we presented unambiguous evidence of ultrafast energy transfer process involving hot electrons or holes at solid/liquid interfaces. Extension of the methodology to the femtosecond time region allowed the observation of ultrafast energy transfer by hot carriers. In particular, the fs-TRG method achieved the observation of interfacial ultrafast energy transfer with high S/N ratio. This owes to the principle of the TRG method and to the fabrication of the sample cell. By extending the TRG method to spectrometry using continuous wavelength light as a probe source, the information on both electronic interaction and thermal energy transfer was obtained spectroscopically. Although its time resolution is on the order of femtosecond, this method has advantages in the measurements of whole ener-

gy transfer process on an extensive time scale from femtosecond to picosecond. We believe that this kind of work using ultrafast photothermal spectroscopy will contribute significantly to the knowledge of interfacial physical chemistry. Especially, the recently developed multiwave femtosecond TRG method using a white light as a probe beam will allow us to obtain more detailed information on ultrafast dynamics involving hot carriers and concerning mechanisms of photocatalytic reactions and so on.

ACKNOWLEDGMENTS

This work was supported by Grant-in-Aids for Specially Promoted Research (No. 07102004) and for Scientific Research on Priority Area of Electrochemistry of Ordered Interfaces (No. 09237219) from the Ministry of Education, Science, and Culture of Japan.

REFERENCES

1. *Photothermal Investigations of Solids and Fluids*, J. A. Sell (Ed.), Academic Press, New York (1989).
2. For example, *11th Int. Conf. on Photoacoustic and Photothermal Phenomena*, T. Sawada (Ed.), *Anal. Sci.* (Special Issue) (2001).
3. *Proc. 10th Int. Topical Meeting on Photoacoustic and Photothermal Phenomena*, F. Scudier (Ed.) (1998).
4. M. Tokeshi, M. Uchida, A. Hibara, T. Sawada, T. Kitamori. *Anal. Chem*. **73**, 2112 (2001).
5. K. Mawatari, T. Kitamori, T. Sawada. *Anal. Chem.* **70**, 5037 (1998).
6. M. Terazima, M. Takezaki, S. Tamaguchi, N. Hirota. *J. Chem. Phys.* **109**, 603 (1998).
7. A. Harata, H. Nishimaru, T. Sawada. *Appl. Phys. Lett.* **57**, 132 (1990).
8. Q. Shen, A. Harata, T. Sawada. *Jpn. J. Appl. Phys.* **32**, 3628 (1993).
9. A. Hibara, A. Harata, T. Sawada. *Chem. Phys. Lett.* **272**, 1 (1997).
10. Jiaqi. Wu, T. Kitamori, T. Sawada. *Appl. Phys. Lett*. **57**, 22 (1990).
11. R. Miller. In *Time Resolved Spectroscopy*, R. J. H. Clark and R. E. Hester (Eds.), pp. 1–54, Wiley, Chichester (1989).
12. Proc. Combined Conf. 4th Int. Conf. on Phonon Phys. and the 8th Int. Conf. on Phonon Scattering in Condensed Matter (1995), *Physica B.,* Vol. 219 (1996).
13. C. B. Harris, N. H. Ge, R. L. Lingle, J. D. Mcneill, Cm. Wong. *Annu. Rev. Phys. Chem.* **48**, 711 (1997).
14. J. W. Gadzuk. In *Femtosecond Chemistry*, J. Manz and L. Wöste (Eds.), p. 603, VCH, Weinheim (1995).
15. A. Harata, N. Adachi, T. Sawada. *Phys. Rev. B.* **58**, 7319 (1998).
16. A. Harata, H. Nishimura, T. Tanaka, T. Sawada. *Rev. Sci. Instrum*. **64**, 618 (1993).
17. A. Harata, Q. Shen, T. Sawada. *Annual Rev. Phys. Chem.* **50**, 193 (1999).
18. S. D. Brorson, J. G. Fujimoto, E. P. Ippen. *Phys. Rev. Lett.* **59**, 1962 (1987).
19. T. Morishita, A. Hibara, T. Sawada, I. Tsuyumoto. *J. Phys. Chem. B.* **103**, 5984 (1999).
20. K. Katayama, Y. Inagaki, T. Sawada. *Phys. Rev. B.* **61**, 7332 (2000).
21. M. Welkowsky and R. Braunstein. *Solid State Commun*. **9**, 2139 (1971).
22. R. Rosei, F. Antonangeli, U. M. Grassano. *Sur. Sci.* **37**, 689 (1973).
23. M. Guerrisi, R. Rosei, P. Winsemius. *Phys. Rev. B.* **12**, 557 (1975).
24. P. Winsemius, M. Guerrisi, R. Rosei. *Phys. Rev. B.* **12**, 4570 (1975).
25. J. Hohlfeld, J. G. Muller, S. S. Wellershoff, E. Matthias. *Appl. Phys. B.* **64**, 387 (1997).
26. R. H. M. Groeneveld, R. Sprik, A. Lagendijk. *Phys. Rev. B* **51**, 5079 (1992).
27. R. H. M. Groeneveld, R. Sprik, A. Lagendijk. *Phys. Rev. B* **51**, 11433 (1995).